

ASAT: Adaptively Scaled Adversarial Training in Time Series

Zhiyuan Zhang
zzy1210@pku.edu.cn
Peking University, China

Wei Li
liweitj47@pku.edu.cn
Peking University, China

Ruihan Bao
ruihan.bao@mizuho-sc.com
Mizuho Securities Co.,Ltd, Japan

Keiko Harimoto
keiko.harimoto@mizuho-sc.com
Mizuho Securities Co.,Ltd, Japan

Yunfang Wu
wuyf@pku.edu.cn
Peking University, China

Xu Sun
xusun@pku.edu.cn
Peking University, China

ABSTRACT

Adversarial training is a method for enhancing neural networks to improve the robustness against adversarial examples. Besides the security concerns of potential adversarial examples, adversarial training can also improve the performance of the neural networks, train robust neural networks, and provide interpretability for neural networks. In this work, we take the first step to introduce adversarial training in time series analysis by taking the finance field as an example. Rethinking existing researches of adversarial training, we propose the adaptively scaled adversarial training (ASAT) in time series analysis, by treating data at different time slots with time-dependent importance weights. Experimental results show that the proposed ASAT can improve both the accuracy and the adversarial robustness of neural networks. Besides enhancing neural networks, we also propose the dimension-wise adversarial sensitivity indicator to probe the sensitivities and importance of input dimensions. With the proposed indicator, we can explain the decision bases of black box neural networks.

CCS CONCEPTS

• **Computing methodologies** → **Neural networks.**

KEYWORDS

time series, adversarial examples, adversarial training

ACM Reference Format:

Zhiyuan Zhang, Wei Li, Ruihan Bao, Keiko Harimoto, Yunfang Wu, and Xu Sun. 2021. ASAT: Adaptively Scaled Adversarial Training in Time Series. In *KDD '21 Workshop on Machine Learning in Finance, August, 2021, Virtual Workshop*. ACM, New York, NY, USA, 11 pages. <https://doi.org/1122445.1122456>

1 INTRODUCTION

Neural networks are found vulnerable to adversarial examples [13, 20, 29, 33] despite their promising performance. Adversarial examples are generated by adding small malicious perturbations to the input data that can mislead models, which reveal the vulnerability

of neural networks with respect to the input data. Adversarial training [6, 13, 30, 38, 42] is a method for enhancing neural networks that can improve both the adversarial robustness and the generalization ability at the same time. Besides the security concerns that neural network faces potential risks of adversarial example attack, researches on adversarial training focus on improving the accuracy of the neural networks [30, 38, 42], training robust neural networks [10, 11, 22], and providing interpretability for neural networks [19, 28, 33].

Traditional adversarial training methods adopt the L_p -norm constraint that treats every dimension of perturbations symmetrically. Rethinking the shift-invariant hypothesis [8, 39] of convolution neural networks in the computer vision (CV) field and the equivalence of different dimensions of word embeddings in the natural language processing (NLP) field [12, 42], it is roughly reasonable that every dimension of the input data is treated as of similar significance by the L_p -norm constraint in adversarial training methods. However, in time series, different dimensions of inputs are not symmetrical. Therefore, we propose to adopt a constraint with adaptive scales according to the importance of different dimensions in time series.

In our work, we propose the adaptively scaled adversarial training (ASAT) in time series analysis in the finance field. The main aim of our work is to improve the generalization ability of neural networks. Visual analysis shows that ASAT can alleviate overfitting to false clues, as shown in Sec. 5.3. Existing researches on adversarial training mainly focus on the CV [13, 30, 33, 38] and NLP [10, 11, 22, 42] fields. To the best of our knowledge, we take the first step towards adversarial training in time series analysis or the finance field.

To validate the effects of ASAT, we implement some representative baselines on a representative time series task on the volume prediction task in the finance field, including moving baselines and several neural network baselines. Among them, we introduce a strong baseline, the Transformer model [35], in volume prediction for the first time. Experimental results show that ASAT can improve the accuracy of neural networks significantly, and can improve the adversarial robustness of neural networks with a big gap.

Besides enhancing neural networks, we also try to explain the decision bases of black box neural networks towards more interpretability for neural network decisions via the proposed dimension-wise adversarial sensitivity indicator. The dimension-wise adversarial sensitivity indicator can reveal the importance of any input dimension in the decision process and help us understand the decision bases of neural networks. A traditional method for interpreting decisions of linear models is factor analysis, where factor loading [3]

Permission to make digital or hard copies of all or part of this work for personal or classroom use is granted without fee provided that copies are not made or distributed for profit or commercial advantage and that copies bear this notice and the full citation on the first page. Copyrights for components of this work owned by others than ACM must be honored. Abstracting with credit is permitted. To copy otherwise, or republish, to post on servers or to redistribute to lists, requires prior specific permission and/or a fee. Request permissions from permissions@acm.org.

KDD '21 workshop, August, 2021, Virtual Workshop

© 2021 Association for Computing Machinery.

ACM ISBN 978-x-xxxx-xxxx-x/YY/MM... \$15.00

<https://doi.org/1122445.1122456>

is adopted to measure the importance of a factor. The weights of the linear model can be seen as the factor loadings roughly. We prove that the proposed sensitivity is proportional to the absolute value of the weight or the factor loading in the linear model, which indicates that the proposed indicator covers traditional measurements. Moreover, in the nonlinear neural networks, the proposed indicator can also probe the importance of input data dimensions.

With the proposed indicator, we have some interesting findings: (1) *ASAT can alleviate overfitting*. As analyzed in Sec. 5.3, baseline models with ASAT are sensitive to different dimensions during multiple training, which indicates that baseline models tend to overfit to some false clues, while ASAT can alleviate it. (2) *ASAT can help models capture fluctuations in time series*. As analyzed in Sec. 5.4, we make detailed examinations on a single data instance and find that ASAT can help models to be more sensitive to abnormal fluctuations. The decision bases of models tend to be more reasonable with ASAT. (3) *Models tend to pay close attention to the volumes of recent time slots*. Models tend to be sensitive to volumes of recent time slots. Since recent time slots are more important in time series regularization, it is reasonable and also accords with human intuition.

Our contributions are summarized as follows:

- To the best of our knowledge, we are the first to propose to apply adversarial training in time series analysis or the finance field to improve both the adversarial robustness and accuracy of neural networks. Rethinking existing adversarial training approaches, we propose to rescale dimensions of the perturbation according to their importance, and propose the adaptively scaled adversarial training (ASAT) algorithm.
- We adopt ASAT on various baselines, including our newly proposed Transformer baselines. Results show that ASAT can improve both the adversarial robustness and accuracy of neural networks.
- With the proposed dimension-wise adversarial sensitivity indicator, we probe the sensitivities of different input dimensions and explain the decision bases of black box neural networks, which provides more interpretability for neural network decisions.

2 ADVERSARIAL TRAINING

In this section, we first introduce the concept of adversarial examples and adversarial training. Then, we describe the proposed dimension-wise adversarial sensitivity indicator inspired by adversarial examples.

2.1 Adversarial Examples

Let \mathcal{D} denote the dataset, $\mathbf{x} = (x_1, x_2, \dots, x_k)^T \in \mathbb{R}^k$ and y stand for a data input and its ground truth. f denote the neural network with the parameter vector θ and \mathcal{L} denote the loss function. The **adversarial example** [13, 33] can be defined as the small perturbation $\delta = (\delta_1, \delta_2, \dots, \delta_k)^T \in \mathbb{R}^k$ on the data input \mathbf{x} that can mislead the model and cause the maximum increases in the loss function,

$$\delta = \arg \max_{\delta \in S} \mathcal{L}(f(\mathbf{x} + \delta, \theta), y) \quad (1)$$

where S denotes the **constraint set**, the perturbation is specified by S . For example, $S = \{\delta : \|\delta\|_2 \leq \epsilon\}$ specifies that the perturbation should be in a k -dimensional hyperball with a radius of ϵ . Typical constraints are L_p -norm bounded and $S = \{\delta : \|\delta\|_p \leq \epsilon\}$, where

$$\|\delta\|_p = \left(\sum_{i=0}^k |\delta_i|^p \right)^{\frac{1}{p}}, \quad \|\delta\|_{+\infty} = \lim_{p \rightarrow +\infty} \|\delta\|_p = \max_{1 \leq i \leq k} |\delta_i| \quad (2)$$

Since neural networks are sensitive to malicious perturbations in inputs, *i.e.*, **adversarial attacks**, the loss increases or accuracy decreases caused by adversarial attacks can evaluate the robustness of neural networks with respect to adversarial attacks, *i.e.*, the **adversarial sensitivity** or the **adversarial robustness**. The adversarial robustness or sensitivity can be defined as,

$$\mathcal{R}(\epsilon) := \mathbb{E} \left[\max_{\delta \in S} \mathcal{L}(f(\mathbf{x} + \delta, \theta), y) - \mathcal{L}(f(\mathbf{x}, \theta), y) \right] \quad (3)$$

To generate adversarial examples, the fast gradient sign method (FGSM) [13] proposes to optimize Eq.(1) via optimizing the first-order Taylor Expansion term of the loss function instead when $S = \{\delta : \|\delta\|_p \leq \epsilon\}$, namely maximizing the inner product of δ and the gradient $\mathbf{g} = \nabla_{\mathbf{x}} \mathcal{L}(f(\mathbf{x}, \theta), y)$,

$$\delta = \arg \max_{\delta \in S} \delta^T \mathbf{g} = \epsilon \operatorname{sgn}(\mathbf{g}) \odot \frac{|\mathbf{g}|^{\frac{1}{p-1}}}{\|\mathbf{g}\|_p^{\frac{1}{p-1}}} \quad (4)$$

Another representative line of existing studies for generating adversarial examples is PGD-based attacks [26, 36]. Suppose $S = \{\delta : \|\delta\|_p \leq \epsilon\}$. The projected gradient descent (PGD) algorithm optimizes Eq.(1) via a multi-step variant of FGSM [13],

$$\delta_{k+1} = \arg \max_{\delta \in S} \Pi_S(\delta_k + \mathbf{u}_{k+1}) \quad (5)$$

where δ_0 is usually set to the zero vector and \mathbf{u}_k is the k -th update in PGD, which is usually solved in Eq.(4) with the constraint $S_1 = \{\delta : \|\delta\|_p \leq \tau\}$ and the step size is set to τ . $\Pi_S(\mathbf{v})$ is the projection function that projects \mathbf{v} into the set S . In two common cases, L_2 -norm [42] and $L_{+\infty}$ -norm [26], the projection functions are,

$$\Pi_{\{\mathbf{v}: \|\mathbf{v}\|_2 \leq \epsilon\}}(\mathbf{v}) = \min\{\|\mathbf{v}\|_2, \epsilon\} \frac{\mathbf{v}}{\|\mathbf{v}\|_2}, \quad (6)$$

$$\Pi_{\{\mathbf{v}: \|\mathbf{v}\|_{+\infty} \leq \epsilon\}}(\mathbf{v}) = \operatorname{clip}(\mathbf{v}, -\epsilon, \epsilon) \quad (7)$$

2.2 Adversarial Training

Since neural networks are sensitive to adversarial examples, **adversarial training** [6, 13] algorithms are designed to improve both the adversarial robustness and the generalization ability of neural networks. The target of adversarial training is seeking to find the parameter vector θ with lower adversarial sensitivities,

$$\theta = \arg \min_{\theta} \mathbb{E}_{(\mathbf{x}, y) \sim \mathcal{D}} \left[\max_{\delta \in S} \mathcal{L}(f(\mathbf{x} + \delta, \theta), y) \right] \quad (8)$$

Typical adversarial training algorithms generate one or multiple adversarial examples to estimate the risk for adversarial attacks and then minimize the risk. Suppose $\mathbf{x}^* = \mathbf{x} + \delta^*$ denotes the adversarial example the algorithm generates, the target of the adversarial training is to minimize both the clean loss and the adversarial sensitivity or adversarial risk,

$$\theta = \arg \min_{\theta} \mathbb{E}_{(\mathbf{x}, y) \sim \mathcal{D}} \left[\lambda_1 \mathcal{L}(f(\mathbf{x}, \theta), y) + \lambda_2 \mathcal{L}(f(\mathbf{x}^*, \theta), y) \right] \quad (9)$$

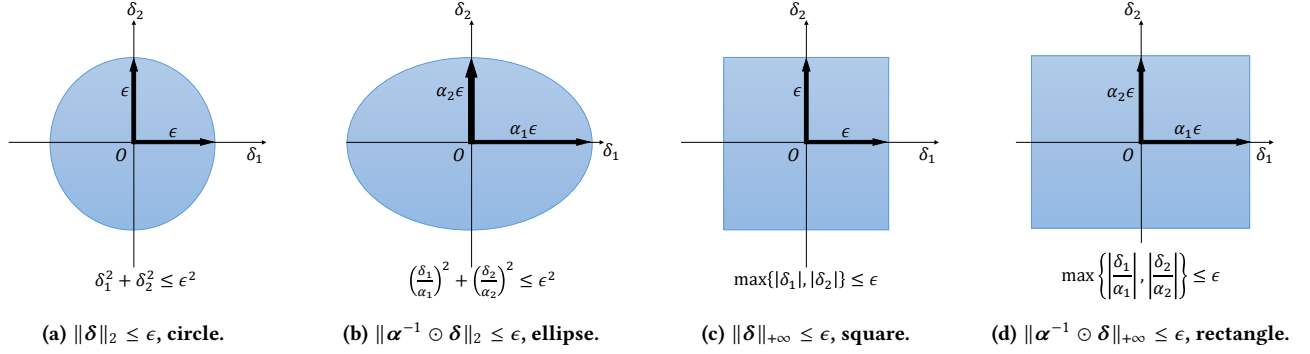


Figure 1: Illustration of the regions that L_2 -norm and $L_{+\infty}$ constraint specify and regions after rescaling.

Goodfellow et al. [13] estimate the risk for adversarial attacks via the FGSM algorithm. Other existing studies also estimate the risk via PGD-based attacks [6, 30, 36, 38, 42]. Besides, some PGD-based adversarial training algorithms [30, 42] minimize the adversarial sensitivities of multiple perturbations generated in different steps.

2.3 Dimension-wise Adversarial Sensitivity

Inspired by the adversarial sensitivity, we propose to probe the sensitivities of different input dimensions and analyze the decision bases of neural networks via dimension-wise adversarial sensitivity. Besides the adversarial sensitivity of the whole model, we can also define the dimension-wise adversarial sensitivity, namely sensitivity of the i -th input dimension. Suppose $\mathcal{R}_i(\epsilon)$ denotes the sensitivities of the i -th dimension, namely the expectation of the maximum loss change when the i -th dimension of the input changes no more than ϵ , which is defined as

$$\mathcal{R}_i(\epsilon) := \mathbb{E} \left[\max_{|\delta_i| \leq \epsilon, \delta_{\neq i} = 0} \mathcal{L}(f(\mathbf{x} + \delta, \theta), y) - \mathcal{L}(f(\mathbf{x}, \theta), y) \right] \quad (10)$$

The sensitivities of input dimensions can reveal the decision basis of the model f and the importance of different dimensions in the process of the prediction process. In traditional factor analysis methods, the factor loading [3] measures the importance of a factor, which can be seen as the weight of the factor in a linear model roughly. The proposed sensitivity does not only cover traditional measurements in the linear model, as illustrated in Proposition 1, but also evaluates the importance of different dimensions in the nonlinear model.

PROPOSITION 1. Consider a linear model $f(\mathbf{x}, \theta) = \theta^T \mathbf{x} + b$. Suppose the loss function $\mathcal{L}(\hat{y}, y)$ is a function $\ell(\hat{y})$ with respect to $\hat{y} = f(\mathbf{x}, \theta)$ and $M = \sup |\ell''|$ exists. Then there exists $C > 0$, such that

$$\mathcal{R}_i(\epsilon) = C\epsilon |\theta_i| + O\left(\frac{M\theta_i^2 \epsilon^2}{2}\right), \quad (i = 1, 2, \dots, k) \quad (11)$$

namely $\mathcal{R}_i(\epsilon) \propto |\theta_i|$ holds approximately when ϵ is small.

Proposition 1 illustrates that the proposed sensitivity is proportional to the absolute value of the weight or the factor loading in a linear model. We put the proof in Appendix. In our work, we adopt the mean squared error (MSE) loss for time series regression tasks, $\mathcal{L}(\hat{y}, y) = (\hat{y} - y)^2$ and $M = 2$.

3 ADVERSARIAL TRAINING IN TIME SERIES

In this section, we first rethink the constraint set in adversarial training. Then, we propose to rescale dimensions of the perturbation in the constraint set. Last, we propose the adaptively scaled adversarial training (ASAT) algorithm.

3.1 Rethinking the Constraint Set in Adversarial Training

Adversarial training algorithms are widely adopted in the CV [6, 13, 33, 38] and NLP [10, 11, 42] fields. The widely-adopted L_p -norm constraint, $S = \{\delta : \|\delta\|_p \leq \epsilon\}$, is invariant about different dimensions of the perturbation, which is reasonable in both the CV and NLP fields.

In the CV field, an important hypothesis of convolution neural networks is shift-invariant [8, 39] and different pixels in an image can be treated of equal significance. In the NLP field, adversarial attacks can be conducted on the word embeddings and different dimensions of word embeddings are of similar significance [12, 42].

However, in time series, different dimensions of inputs are not symmetrical. Therefore, directly adopting the L_p -norm constraint in adversarial training in time series is not reasonable.

3.2 Rescaling the Constraint in Adversarial Training in Time Series

Scales of all dimensions of the L_p -norm bounded constraint are the same. However, in time series, dimensions with different timestamps may be of different significance. The time series is usually defined as $\mathbf{X} = (\mathbf{x}_1, \mathbf{x}_2, \dots, \mathbf{x}_T)$, where \mathbf{x}_t is the input vector at the timestamp t . In our work, we flatten a time series into a vector $\mathbf{x} = (x_1, x_2, \dots, x_k)^T \in \mathbb{R}^k$ and define timestamp i as the timestamp of the i -th dimension.

Suppose $\alpha = (\alpha_1, \alpha_2, \dots, \alpha_k)^T$, we multiply the scale of dimension i of the perturbation with α_i to rescale the radius of dimension i from ϵ to $\alpha_i \epsilon$. As illustrated in Fig. 1, the L_2 -norm bounded constraint specifies a k -dimensional hyperball in \mathbb{R}^k (a circle in \mathbb{R}^2 , as shown in Fig. 1a) and the $L_{+\infty}$ -norm bounded constraint specifies a k -dimensional hypercube in \mathbb{R}^k (a square in \mathbb{R}^2 , as shown in Fig. 1b). After rescaling, the hyperball is transformed to a hyperellipsoid (a ellipse in \mathbb{R}^2 , as shown in Fig. 1c) and the hypercube is transformed

Algorithm 1 Adaptively Scaled Adversarial Training (ASAT) Algorithm

Require: Network f ; parameters $\theta \in \mathbb{R}^k$; loss \mathcal{L} and dataset \mathcal{D} ; constraint set S ; step number K and step size τ ; optimizer \mathcal{O} ; training iterations; batch size $|\mathcal{B}|$.

```

1: Initialize  $\theta$ .
2: while Training do
3:   Generate a batch  $\mathcal{B}$ .
4:   for  $(\mathbf{x}, y) \in \mathcal{B}$  do
5:      $\delta_0 \leftarrow \mathbf{0}_k$ .
6:     Calculate the risk:  $\mathcal{L}(f(\mathbf{x} + \delta_0, \theta), y)$ .
7:     for  $k = 1$  to  $K$  do
8:       Generate  $\mathbf{u}_k$  according to Eq.(13) with step size  $\tau$ .
9:       Generate  $\delta_k$  by projecting  $\delta_{k-1} + \mathbf{u}_k$  to the constraint set  $S$  according to Eq.(5), Eq.(14) and Eq.(15).
10:      Calculate the risk:  $\mathcal{L}(f(\mathbf{x} + \delta_k, \theta), y)$ .
11:    end for
12:  end for
13:  Update  $\theta$  with optimizer  $\mathcal{O}$  according to Eq.(16).
14: end while

```

to a hypercuboid (a rectangle in \mathbb{R}^2 , as shown in Fig. 1d). The rescaling process assigns different importance to different dimensions of perturbations in adversarial training. Generally, the L_p -norm constraint $\|\delta\|_p \leq \epsilon$ is transformed to the constraint,

$$\|\alpha^{-1} \odot \delta\|_p = \left(\sum_{i=1}^k \left| \frac{\delta_i}{\alpha_i} \right|^p \right)^{\frac{1}{p}} \leq \epsilon \quad (12)$$

3.3 FGSM and PGD Algorithms after Rescaling

After rescaling, the constraint set is $S = \{\delta : \|\alpha^{-1} \odot \delta\|_p \leq \epsilon\}$. For the FGSM target, namely maximizing the inner product of δ and the gradient \mathbf{g} , the solution Eq.(4) becomes,

$$\delta = \arg \max_{\delta \in S} \delta^T \mathbf{g} = \epsilon (\alpha \odot \text{sgn}(\mathbf{g})) \odot \frac{|\alpha \odot \mathbf{g}|^{\frac{1}{p-1}}}{\|\alpha \odot \mathbf{g}\|_p^{\frac{1}{p-1}}} \quad (13)$$

For the projection function $\Pi_S(\mathbf{v})$ that projects \mathbf{v} into the set S , we adopt the variants of Eq.(6) and Eq.(7),

$$\Pi_{\{\mathbf{v}: \|\alpha^{-1} \odot \mathbf{v}\|_2 \leq \epsilon\}}(\mathbf{v}) = \min\{\|\alpha^{-1} \odot \mathbf{v}\|_2, \epsilon\} \frac{\mathbf{v}}{\|\alpha^{-1} \odot \mathbf{v}\|_2} \quad (14)$$

$$\Pi_{\{\mathbf{v}: \|\alpha^{-1} \odot \mathbf{v}\|_{+\infty} \leq \epsilon\}}(\mathbf{v}) = \alpha \odot \text{clip}(\alpha^{-1} \odot \mathbf{v}, -\epsilon, \epsilon) \quad (15)$$

The proof and theoretical details are in Appendix.

3.4 Adaptively Scaled Adversarial Training

To rescale different dimensions of perturbations in adversarial training, we propose the adaptively scaled adversarial training (ASAT) algorithm, as illustrated in Algorithm 1. The target of the proposed algorithm is minimizing both the clean loss and the adversarial sensitivity. Following Zhu et al. [42], we optimize the risk on a batch \mathcal{B} by minimizing the average risks of multiple adversarial

Table 1: Statistical information on the two datasets.

Dataset	Hourly			Five-minute		
	Train	Dev	Test	Train	Dev	Test
Samples	49,728	16,554	26,818	106,784	35,552	27,584

examples generated during PGD process,

$$\theta = \arg \min_{\theta} \mathbb{E}_{(\mathbf{x}, y) \in \mathcal{B}} \left[\frac{1}{K+1} \sum_{k=0}^K \mathcal{L}(f(\mathbf{x} + \delta_k, \theta), y) \right] \quad (16)$$

In the constraint set $S = \{\delta : \|\alpha^{-1} \odot \delta\|_p \leq \epsilon\}$, we rescale the dimension i with α_i adaptively according to timestamp $_i$. Suppose t_i denotes that timestamp $_i$ is the t_i -th latest timestamp (we only consider unique timestamps), we set $\alpha_i = \alpha(t_i)$, where $\alpha : \mathbb{N}_+ \rightarrow [0, 1]$ is a function that calculates the scales of different timestamps. Since in time series analysis, data of closer timestamps may be more important, We may assume $\alpha(t) \geq \alpha(t+1)$ and $\alpha(1) = 1$. The scale $\alpha(t)$ decays when t increases.

We consider three simple decay functions:

- **Constant (Const).** $\alpha(t) = 1$.
- **Exponential Decay (Exp).** $\alpha(t) = \gamma^{t-1}$.
- **Linear Decay (Linear).** $\alpha(t) = 1 - (1 - \gamma) \times \frac{t-1}{T-1}$.

where the hyperparameter $\gamma \in (0, 1]$ controls the decaying speed. When $\gamma = 1$, decay functions degrade to constant. T denotes the maximum value of t_i , i.e., the number of different timestamps. For other complex decay functions, more hyperparameters may be involved. It is costly for hyperparameter tuning for other complex decay functions involving more hyperparameters. Therefore, we only consider three simple decay functions, the constant, exponential decay, and linear decay functions, in our work and empirically adopt the exponential decay function.

4 EXPERIMENTS

In this section, we first introduce the task and dataset details, then introduce the baseline models and experimental settings. Last, we report experimental results and conduct statistical tests.

4.1 Tasks and Datasets

4.1.1 Volume prediction task. We choose the volume prediction task, the input data consists of log prices and log volumes of previous 12 time slots and the same time slots in previous 20 trading days. The prices include open, close, high, and low prices. The input data consists of 32×4 log prices and 32×1 log volumes totally. The target is to regress the log volume. In our experiments, the values of t of i -th nearest time slots and the j -th nearest day in history are i and j , respectively.

4.1.2 Datasets and data preprocessing. For our research, we adopt the **hourly** inter-day volume prediction dataset and the **five-minute** intra-day volume prediction dataset. The two datasets are extracted from the price and volume data of the Topix500 (price index of the 500 most liquid and highly market capitalized stocks in Tokyo Stock) between *Jan. 2017* and *Feb. 2018*. We adopt the data of *2017* as the training set and development set, and the data of *Jan. 2018* and *Feb. 2018* as the test set. The training set and the development set

Table 2: Experimental results of moving average baselines and neural network baselines. All t -values are larger than 1.943 and the proposed ASAT outperforms baselines statistically significantly ($p < 0.05$) except the t -value marked with #.

Dataset	Hourly				Five-minute			
Model	MSE	RMSE	MAE	ACC	MSE	RMSE	MAE	ACC
yesterday	0.286	0.535	0.406	0.689	1.205	1.098	0.797	0.666
20-day average	0.249	0.499	0.385	0.710	0.700	0.837	0.608	0.709
20-day EMA	0.288	0.536	0.413	0.696	0.808	0.899	0.659	0.692
last time slot	0.324	0.569	0.439	0.500	1.125	1.060	0.745	0.500
12-slot average	0.524	0.724	0.413	0.696	0.988	0.994	0.714	0.629
12-slot EMA	0.331	0.575	0.443	0.642	1.314	1.146	0.844	0.602
20-day and 12-slot average	0.271	0.521	0.393	0.662	0.741	0.861	0.609	0.695
Linear	0.227±0.019	0.477±0.019	0.370±0.023	0.708±0.012	0.808±0.072	0.892±0.041	0.700±0.029	0.660±0.037
+ASAT	0.206±0.004	0.454±0.005	0.344±0.006	0.722±0.006	0.675±0.061	0.820±0.037	0.622±0.047	0.693±0.027
t -values	2.163	2.341	2.188	2.087	2.819	2.607	2.825	2.751
LSTM	0.220±0.001	0.470±0.001	0.358±0.003	0.708±0.004	0.797±0.019	0.892±0.011	0.690±0.013	0.671±0.006
+ASAT	0.217±0.002	0.467±0.002	0.354±0.002	0.714±0.003	0.756±0.015	0.870±0.008	0.675±0.012	0.673±0.005
t -values	2.683	2.683	2.219	2.400	3.387	3.235	2.826	0.512 [#]
Transformer	0.219±0.012	0.470±0.013	0.357±0.012	0.711±0.012	0.665±0.044	0.815±0.027	0.610±0.032	0.695±0.019
+ASAT	0.205±0.005	0.453±0.005	0.343±0.004	0.724±0.005	0.613±0.028	0.783±0.018	0.571±0.018	0.717±0.007
t -values	2.154	3.303	2.214	2.000	1.994	1.972	2.124	2.713

are randomly split with the ratio of 3 : 1. The statistics of datasets are in Table 1.

For example, in the hourly dataset, if the ground truth is the log volume of 10:00-11:00, Jan. 21, then the previous 12 time slots are: 9:00-10:00, Jan. 21, 14:00-15:00, Jan. 20, etc, and the history 20 days are: 10:00-11:00, Jan. 20, 10:00-11:00, Jan. 19, etc. It is similar in data preprocessing of the five-minute dataset. We deleted the data instances consisting of missing volumes or prices. In the five-minute dataset, the previous 12 time slots are collected from the same day to the ground truth.

4.1.3 Evaluation metrics. We adopt four evaluation metrics: mean squared error (MSE), root mean squared error (RMSE), mean absolute error (MAE), and accuracy (ACC). Suppose $\hat{y} = f(\mathbf{x}, \theta)$ and y is the ground truth, then these metrics are defined as,

$$\text{MSE} = \mathbb{E}_{(\mathbf{x}, y) \sim \mathcal{D}} (\hat{y} - y)^2 \quad (17)$$

$$\text{RMSE} = \sqrt{\mathbb{E}_{(\mathbf{x}, y) \sim \mathcal{D}} (\hat{y} - y)^2} \quad (18)$$

$$\text{MAE} = \mathbb{E}_{(\mathbf{x}, y) \sim \mathcal{D}} |\hat{y} - y| \quad (19)$$

$$\text{ACC} = \mathbb{P}_{(\mathbf{x}, y) \sim \mathcal{D}} ((\hat{y} - x_{\text{last}}) \times (y - x_{\text{last}}) > 0) \quad (20)$$

here x_{last} denotes the volume of the last time slot, ACC is the accuracy of whether the volume increases or decreases compared to the last time slot.

4.2 Baselines

We implement multiple moving average baselines and three neural network baselines in our experiments.

4.2.1 Moving average baselines. We adopt moving average baselines as our baselines, which are commonly used in technical analysis in finance. In statistics, suppose a series x_1, x_2, \dots, x_T , three commonly adopted estimations are:

- **Naive forecasting.** The naive forecasting algorithm uses x_T as the prediction. In our experiments, we try to adopt the volumes of **yesterday** or **last time slot** as the prediction.

- **Simple moving average (SMA).** SMA uses the average value $\bar{x} = \frac{1}{T} \sum_{i=1}^T x_i$ as the prediction. In our experiments, we try to adopt the volumes of **20-day average** or **12-slot average** as the prediction.
- **Exponential moving average (EMA).** EMA places a greater weight on the nearest values. It sets $y_1 = x_1$, $y_t = (1 - \rho)y_{t-1} + \rho x_t$ and uses y_T as the prediction. In our experiments, we adopt $\rho = 0.04$ and try to use the **20-day EMA** or **12-slot EMA** as the prediction.

We also try a method that considers both the 20-day average and 12-slot average volumes, **20-day and 12-slot average**. It uses the mean of 20-day average and 12-slot average as the prediction.

4.2.2 Linear. The linear model is formulated as $f(\mathbf{x}, \theta) = \theta^T \mathbf{x} + b$, where $\mathbf{x} \in \mathbb{R}^{160}$ is the flattened vector of the concatenated input of both 12-slot and 20-day history.

4.2.3 LSTM. The long-short term memory (LSTM) [15] networks can capture features and long-term dependency in the entire sequences of data. Following Libman et al. [23], we implement two one-layer LSTM models with the global attention mechanism [25] to generate the representation vectors of previous time slots and 20-day history. Before feeding input into LSTM, we first adopt two linear layers to project the inputs into two higher dimensional spaces, respectively. Then, we concatenate the representation vectors and feed them into a linear layer to regress the log volume. The input size, hidden size, and output size of LSTM models are 200.

4.2.4 Transformer. We also implement a six-layer Transformer [35] encoder model as a baseline. We concatenate the 12-slot and 20-day history input and add a special token [CLS] before it to get a series $\mathbf{X} \in \mathbb{R}^{33 \times 5}$. The data of [CLS], $\mathbf{X}[0, :]$, is treated as a trainable parameter of Transformer. Before feeding input into Transformer, we first adopt one linear layer to project the inputs into a higher dimensional space. Then, we feed the output representation of [CLS] of the last layer into a linear layer to regress the volume. The input size, hidden size, and output size are 200, where the hidden states are split into 8 heads.

Table 3: Results of different decay functions in adversarial training. Experimental results show that exponential decay function outperforms others.

Dataset	Hourly				Five-minute			
Model	MSE	RMSE	MAE	ACC	MSE	RMSE	MAE	ACC
20-day average	0.249	0.499	0.385	0.710	0.700	0.837	0.608	0.709
Linear	0.227	0.477	0.370	0.708	0.808	0.892	0.700	0.660
w/ Const	0.208	0.456	0.349	0.718	0.669	0.817	0.619	0.692
w/ Linear	0.207	0.455	0.345	0.721	0.695	0.833	0.638	0.684
w/ Exp	0.206	0.454	0.344	0.722	0.675	0.820	0.622	0.693
LSTM	0.220	0.470	0.358	0.708	0.797	0.892	0.690	0.671
w/ Const	0.220	0.469	0.356	0.711	0.783	0.885	0.691	0.670
w/ Linear	0.218	0.467	0.355	0.714	0.790	0.889	0.697	0.665
w/ Exp	0.217	0.467	0.354	0.714	0.756	0.870	0.675	0.673
Transformer	0.219	0.470	0.357	0.711	0.665	0.815	0.610	0.695
w/ Const	0.217	0.461	0.352	0.716	0.620	0.787	0.575	0.715
w/ Linear	0.210	0.456	0.347	0.721	0.625	0.790	0.581	0.711
w/ Exp	0.205	0.453	0.343	0.724	0.613	0.783	0.571	0.717

4.3 Settings and Choices of Hyperparameters

We train every model for 5 epochs and report the test performance on the checkpoint with the lowest valid loss. We adopt the Adam optimizer and initialize the learning rate with 0.001. The batch size is 32. We repeat every experiment with 4 runs. Experiments are conducted on a GeForce GTX TITAN X GPU.

Following Zhu et al. [42], we set $K = 3$ and $\tau = 1.5 * \epsilon / K = \epsilon / 2$ in ASAT, where the hyperparameter K is the step number in ASAT attacks, τ is the step size and ϵ controls the strength of adversarial training in the constraint set S . We try L_2 and $L_{+\infty}$ in S , and grid-search the hyperparameters ϵ and γ in ASAT. The process of hyperparameter search shows that too large or small ϵ cannot improve the model accuracy well, and an appropriate ϵ needs to be selected. For the same ϵ , an appropriate γ needs to be selected too. Detailed experimental results in the choice of hyperparameters are reported in Appendix.

4.4 Experimental Results

After selecting the best configurations of hyperparameters, the experimental results are shown in Table 2. It can be concluded that the 20-day average baseline performs best among multiple moving average baselines and three neural network baselines perform better than the 20-day average baseline. We only report results of the 20-day average baseline in the following analysis. Moreover, the proposed ASAT can improve the performance of baselines.

We also conduct student- t tests to verify that the proposed ASAT outperforms baselines statistically significantly ($p < 0.05$). The degree of freedom is $df=6$ and the critical t -value is 1.943. We can see that all t -values are larger than 1.943 except the t -values of LSTM ACC on the five-minute dataset.

5 ANALYSIS

In this section, we first compare different decay functions. Then, we compare the adversarial robustness of neural networks after ASAT. Last, we probe the sensitivities of different input dimensions and analyze the decision bases of neural networks, both on the dataset level and single instance level.

Table 4: Results of models under adversarial attacks. Experimental results show that ASAT can improve the adversarial robustness of neural networks with a big gap.

Hourly	Clean				w/ attack			
Model	MSE	RMSE	MAE	ACC	MSE	RMSE	MAE	ACC
20-day average	0.249	0.499	0.385	0.710	0.280	0.529	0.421	0.671
Linear	0.227	0.477	0.370	0.708	0.430	0.656	0.581	0.582
+ASAT	0.206	0.454	0.344	0.722	0.349	0.591	0.516	0.584
LSTM	0.220	0.470	0.358	0.722	0.301	0.548	0.455	0.635
+ASAT	0.217	0.467	0.354	0.714	0.259	0.508	0.407	0.681
Transformer	0.219	0.470	0.357	0.711	0.411	0.641	0.517	0.633
+ASAT	0.205	0.453	0.343	0.724	0.338	0.582	0.459	0.652

Five-minute	Clean				w/ attack			
Model	MSE	RMSE	MAE	ACC	MSE	RMSE	MAE	ACC
20-day average	0.700	0.837	0.608	0.709	0.834	0.913	0.711	0.674
Linear	0.808	0.892	0.700	0.660	1.580	1.257	1.114	0.503
+ASAT	0.675	0.820	0.622	0.693	0.778	0.882	0.703	0.655
LSTM	0.797	0.892	0.690	0.671	1.006	1.003	0.824	0.620
+ASAT	0.756	0.870	0.675	0.673	0.815	0.903	0.716	0.651
Transformer	0.665	0.815	0.610	0.695	0.915	0.956	0.762	0.627
+ASAT	0.613	0.783	0.571	0.717	0.720	0.848	0.644	0.690

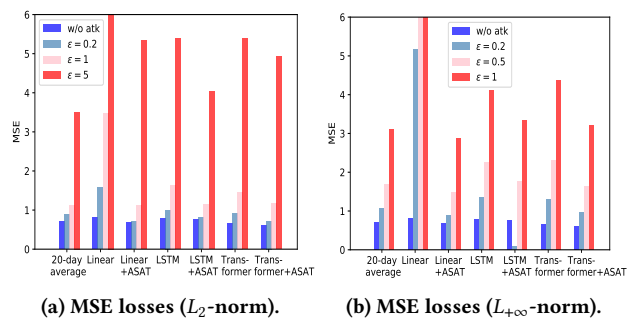


Figure 2: MSE losses of models under multiple adversarial attacks with L_2 -norm and $L_{+\infty}$ -norm constraints. MSE losses larger than 6 are not completely shown. Results show that ASAT can improve the adversarial robustness of models with a big gap.

5.1 Comparisons of Decay Functions

We conduct an ablation study to investigate the influence of different decay functions. Experimental results are shown in Table 3.

Experimental results show that the exponential decay function outperforms others in most cases. Generally speaking, adversarial training can improve the generalization ability of baseline models, which illustrates the effectiveness of adversarial training. Linear and exponential decay functions outperform the constant decay function, which indicates that our proposed ASAT algorithm outperforms conventional adversarial training widely adopted in the CV and NLP fields. Among linear and exponential decay functions, the exponential decay function performs best.

5.2 Adversarial Robustness with ASAT

We compare the adversarial robustness of baseline models and ASAT models under multiple adversarial attacks.

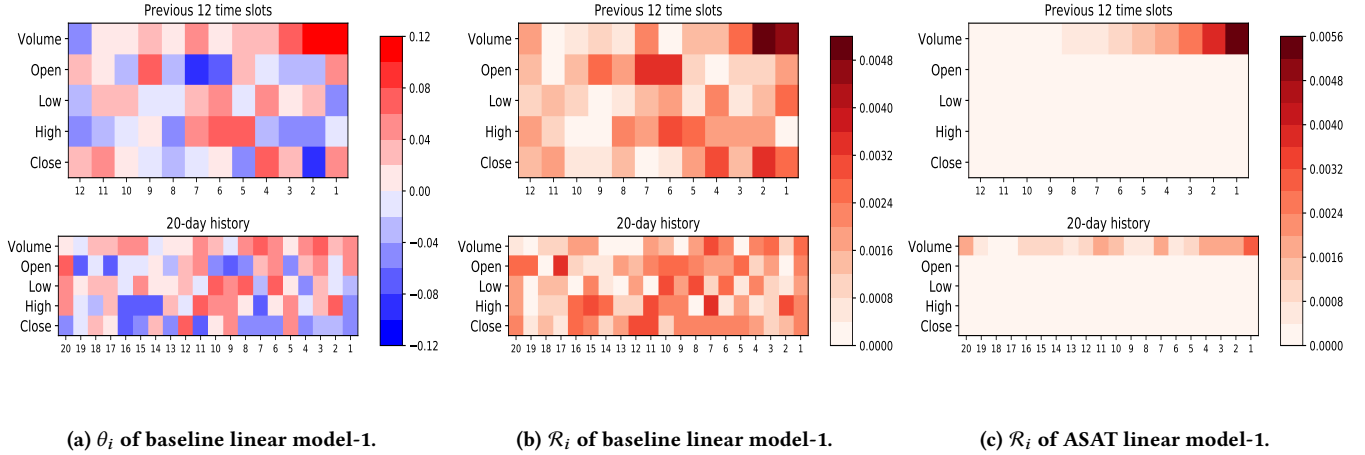


Figure 3: Weights θ_i and sensitivities \mathcal{R}_i of linear models, both baseline and model with ASAT, on the dataset. The sensitivity of the linear model is proportional to the absolute value of the weight or the factor loading in a linear model.

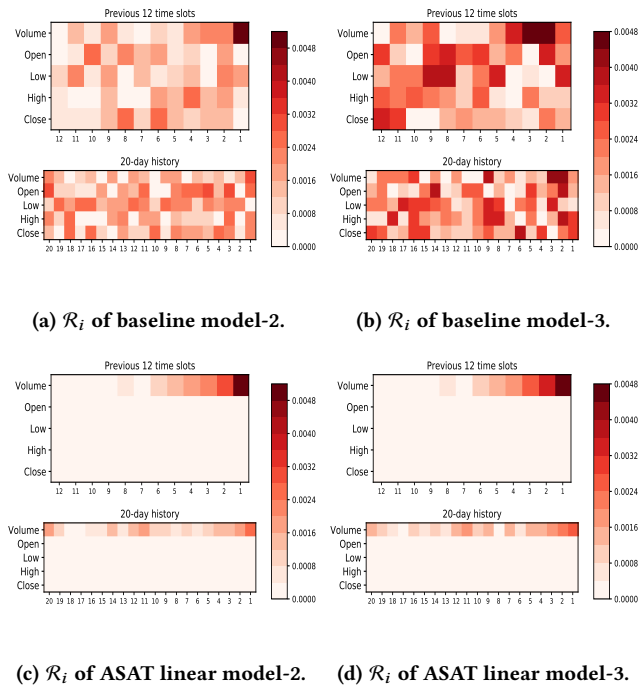


Figure 4: Visualization of the sensitivities of two baseline linear models and two linear models with ASAT, on the dataset. Baseline models are sensitive to different dimensions during multiple training and tend to overfit to some false clues while ASAT can alleviate the overfitting since models with ASAT always focus on similar dimensions.

We first choose an L_2 -norm constraint attack with $\epsilon = 0.2$ and report the clean performance and performance with attack (w/ attack) of models. Results are shown in Table 4. Experimental results

show that ASAT can improve the adversarial robustness of models with a big gap. Moreover, baseline linear, LSTM and Transformer models tend to be more sensitive to adversarial attacks than the 20-day average, which indicates that the traditional 20-day average baseline is more robust than neural networks. However, ASAT can improve the robustness of neural networks and achieve similar robustness to the 20-day average.

We also conduct multiple adversarial attacks on models on the five-minute dataset. Experimental results are shown in Figure 2. Similarly, we can conclude that ASAT can improve the adversarial robustness of models with a big gap.

5.3 Probing Sensitivities of Input Dimensions

We probe the sensitivities of different input dimensions in linear models, trained with three random seeds, the visualization results are shown in Fig. 3 and Fig. 4. Here we choose the five-minute dataset, $\epsilon = 1$, and the sensitivities are defined on the whole dataset.

As shown in Fig. 3a and Fig. 3b, the sensitivity of the linear model is proportional to the absolute value of the weight or the factor loading in a linear model, which accords with the theoretical results in Proposition 1 that the adversarial sensitivity of a single dimension in linear models can reflect the absolute value of the weight or the factor loading.

Fig. 3b, Fig. 4a and Fig. 4b show the sensitivities of baseline linear models with three random seeds. The dimensions models pay close attention to are different during multiple training, which indicates that baseline linear models tend to overfit to some false clues. However, as shown in Fig. 3c, Fig. 4c and Fig. 4d, models with ASAT often pay close attention to some recent time slots and are sensitive to them, which accords with human intuition and is reasonable since recent time slots are more important in time series regularization. It also indicates that ASAT can alleviate the overfitting since models with ASAT often focus on similar dimensions during multiple training.

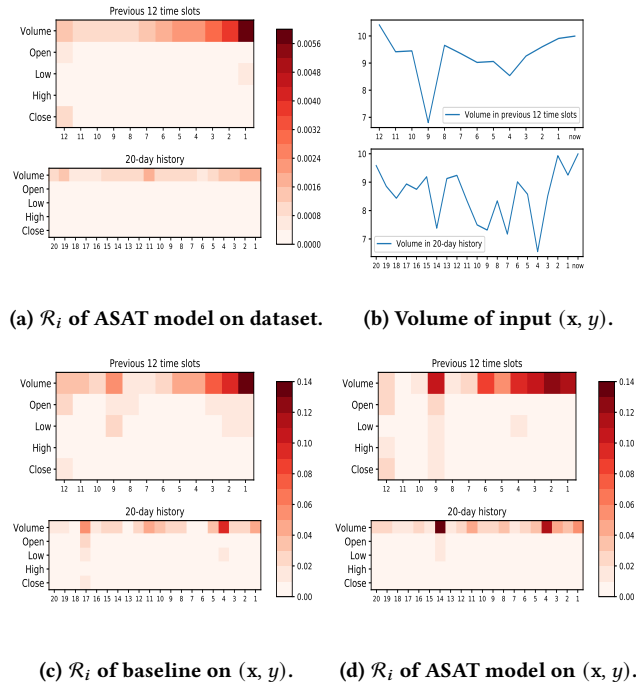


Figure 5: Visualization of the sensitivities of transformer models, which reveals that models can capture abnormal fluctuations on the data input.

5.4 Analysing Decision Basis on Individual Instance

In Eq.(10), the sensitivity can be defined on a dataset \mathcal{D} or a single data instance (x, y) . When it is defined on a single instance, it can be adopted to probe the decision basis on a single instance. This probing method can provide more interpretability for neural network decisions, and provide insights on explaining the decision basis of a black box model, both on a dataset or an input.

We choose the five-minute dataset, $\epsilon = 1$, and randomly choose a data instance in the dataset to plot the sensitivities on the dataset and on a single data instance. As shown in Fig. 5, Fig. 5a shows the sensitivities of a Transformer model trained with ASAT on the dataset. We can see that the model mainly concerns the volumes of nearest time slots and volumes in 20-day history. We also probe the decision basis on the data instance, whose volumes are shown in Fig. 5b. The volumes of the 9-th nearest time slots, the 14-th nearest day in history, and the 4-th nearest day in history are relatively low compared to other time slots or days in history. Both the baseline Transformer (shown in Fig. 5c) and the ASAT Transformer (shown in Fig. 5d) are sensitive to these time slots or days. They pay close attention to these abnormal volumes and the corresponding prices. Therefore, their decisions on this data instance can capture these abnormal fluctuations. It can also be concluded that Transformer is a strong baseline and it outperforms other neural network models. Moreover, the model with ASAT tends to be more sensitive to abnormal fluctuations, which indicates that ASAT can help the decision bases of models be more reasonable.

A potential negative societal impact is that malicious attackers may attack financial models or analyze the decision bias of financial models for plagiarizing trade secrets, with the proposed indicator. Therefore, we call on financial model providers to only provide black box models to defend the potential attacks or plagiarism, since the calculation of the proposed indicator requires gradients.

6 RELATED WORK

6.1 Adversarial Training

Szegedy et al. [33] first propose the concept of adversarial examples that can mislead deep neural networks with small malicious perturbations, even in the physical world scenarios [20]. Besides generating adversarial examples to attack models [6, 12, 13, 20, 21, 29, 32, 33], existing studies also concern improving the adversarial robustness and generalization ability of neural networks via adversarial training [6, 13, 30, 38, 42]. Adversarial training is widely adopted in both the computer vision field [6, 13, 30, 31, 38, 41] and the natural language processing field [10, 11, 22, 40, 42]. To the best of our knowledge, we are the first to propose to apply adversarial training in time series analysis or the finance field.

6.2 Time Series Analysis and Volume Prediction

Trading volume prediction plays an important role in algorithmic trading strategies [4, 5, 7, 14, 18, 27, 43]. Many efforts are paid to volume prediction [1, 2, 9, 16, 17, 23, 24, 34, 37]. Machine learning or deep learning methods have many applications in volume prediction. Liu and Lai [24] propose a dynamic SVM-based approach for volume forecasting and Chen et al. [9] adopt a Kalman filter approach. Libman et al. [23] first adopts LSTM models in volume prediction. Huptas [16] models the volume forecasting task as Bayesian autoregressive conditional models. Antulov-Fantulin et al. [2] proposes temporal mixture ensemble models for volume predictions. To the best of our knowledge, we propose to adopt Transformer [35] in volume prediction for the first time.

7 CONCLUSION AND FUTURE WORK

In this work, we first introduce the adaptively scaled adversarial training (ASAT) to enhance neural networks in time series analysis. The proposed approach adaptively rescales different dimensions of perturbations according to their importance. ASAT can improve both the accuracy and adversarial robustness of several baseline models on intra-day and inter-day volume prediction tasks. We also propose the dimension-wise adversarial sensitivity indicator and utilize it to explain the decision bases of neural networks. In this work, we still use pre-determined decay functions in the scales of dimensions, and the characteristics of different instances have not yet been taken into consideration. In the future, we will investigate an instance-wise adaptively scaled adversarial training method.

ACKNOWLEDGEMENTS

This work is supported by a Research Grant from Mizuho Securities Co., Ltd. We sincerely thank Mizuho Securities for valuable domain expert suggestions. The experiment data is provided by Mizuho Securities and Reuters.

REFERENCES

- [1] LG Alvim, Cicero N dos Santos, and Ruy L Milidui. 2010. Daily volume forecasting using high frequency predictors. In *Proceedings of the 10th IASTED International Conference*, Vol. 674. 248.
- [2] Nino Antulov-Fantulin, Tian Guo, and Fabrizio Lillo. 2020. Temporal mixture ensemble models for intraday volume forecasting in cryptocurrency exchange markets. *arXiv preprint arXiv:2005.09356* (2020).
- [3] Deborah L Bandalos. 2018. *Measurement theory and applications for the social sciences*. Guilford Publications.
- [4] Jędrzej Białkowski, Serge Darolles, and Gaëlle Le Fol. 2008. Improving VWAP strategies: A dynamic volume approach. *Journal of Banking & Finance* 32, 9 (2008), 1709–1722.
- [5] Christian T Brownlees, Fabrizio Cipollini, and Giampiero M Gallo. 2011. Intradaily volume modeling and prediction for algorithmic trading. *Journal of Financial Econometrics* 9, 3 (2011), 489–518.
- [6] Nicholas Carlini and David A. Wagner. 2017. Towards Evaluating the Robustness of Neural Networks. In *2017 IEEE Symposium on Security and Privacy, SP 2017, San Jose, CA, USA, May 22-26, 2017*. 39–57. <https://doi.org/10.1109/SP.2017.49>
- [7] Álvaro Cartea and Sebastian Jaimungal. 2016. A closed-form execution strategy to target volume weighted average price. *SIAM Journal on Financial Mathematics* 7, 1 (2016), 760–785.
- [8] Anadi Chaman and Ivan Dokmanic. 2020. Truly shift-invariant convolutional neural networks. *CoRR abs/2011.14214* (2020). [arXiv:2011.14214](https://arxiv.org/abs/2011.14214) <https://arxiv.org/abs/2011.14214>
- [9] Ran Chen, Yiyong Feng, and Daniel Palomar. 2016. Forecasting intraday trading volume: a kalman filter approach. *Available at SSRN 3101695* (2016).
- [10] Yong Cheng, Lu Jiang, and Wolfgang Macherey. 2019. Robust Neural Machine Translation with Doubly Adversarial Inputs. In *Proceedings of the 57th Annual Meeting of the Association for Computational Linguistics*. Association for Computational Linguistics, Florence, Italy, 4324–4333. <https://doi.org/10.18653/v1/P19-1425>
- [11] Yong Cheng, Lu Jiang, Wolfgang Macherey, and Jacob Eisenstein. 2020. AdvAug: Robust Adversarial Augmentation for Neural Machine Translation. In *Proceedings of the 58th Annual Meeting of the Association for Computational Linguistics*. Association for Computational Linguistics, Online, 5961–5970. <https://doi.org/10.18653/v1/2020.acl-main.529>
- [12] Javid Ebrahimi, Anyi Rao, Daniel Lowd, and Dejing Dou. 2018. HotFlip: White-Box Adversarial Examples for Text Classification. In *Proceedings of the 56th Annual Meeting of the Association for Computational Linguistics, ACL 2018, Melbourne, Australia, July 15-20, 2018, Volume 2: Short Papers*, Iryna Gurevych and Yusuke Miyao (Eds.). Association for Computational Linguistics, 31–36. <https://doi.org/10.18653/v1/P18-2006>
- [13] Ian J. Goodfellow, Jonathon Shlens, and Christian Szegedy. 2015. Explaining and Harnessing Adversarial Examples. In *3rd International Conference on Learning Representations, ICLR 2015, San Diego, CA, USA, May 7-9, 2015, Conference Track Proceedings*.
- [14] Olivier Guéant and Guillaume Royer. 2014. VWAP execution and guaranteed VWAP. *SIAM Journal on Financial Mathematics* 5, 1 (2014), 445–471.
- [15] Sepp Hochreiter and Jürgen Schmidhuber. 1997. Long Short-term Memory. *Neural computation* 9 (12 1997), 1735–80. <https://doi.org/10.1162/neco.1997.9.8.1735>
- [16] Roman Huptas. 2019. Point forecasting of intraday volume using Bayesian autoregressive conditional volume models. *Journal of Forecasting* 38, 4 (2019), 293–310.
- [17] Ryoko Ito. 2016. Spline-DCS for Forecasting Trade Volume in High-Frequency Financial Data. (2016).
- [18] Taisei Kaizoji, Thomas Lux, et al. 2004. *Forecasting volume and volatility in the Tokyo stock market: The advantage of long memory models*. Technical Report. Society for Computational Economics.
- [19] Hamid Karimi, Tyler Derr, and Jiliang Tang. 2019. Characterizing the Decision Boundary of Deep Neural Networks. *CoRR abs/1912.11460* (2019). [arXiv:1912.11460](https://arxiv.org/abs/1912.11460) <http://arxiv.org/abs/1912.11460>
- [20] Alexey Kurakin, Ian J. Goodfellow, and Samy Bengio. 2017. Adversarial examples in the physical world. In *5th International Conference on Learning Representations, ICLR 2017, Toulon, France, April 24-26, 2017, Workshop Track Proceedings*.
- [21] Jinfeng Li, Shouling Ji, Tianyu Du, Bo Li, and Ting Wang. 2019. TextBugger: Generating Adversarial Text Against Real-world Applications. In *26th Annual Network and Distributed System Security Symposium, NDSS 2019, San Diego, California, USA, February 24-27, 2019*. The Internet Society. <https://www.ndss-symposium.org/ndss-paper/textbugger-generating-adversarial-text-against-real-world-applications/>
- [22] Yitong Li, Timothy Baldwin, and Trevor Cohn. 2018. What’s in a Domain? Learning Domain-Robust Text Representations using Adversarial Training. In *Proceedings of the 2018 Conference of the North American Chapter of the Association for Computational Linguistics: Human Language Technologies, NAACL-HLT, New Orleans, Louisiana, USA, June 1-6, 2018, Volume 2 (Short Papers)*, Marilyn A. Walker, Heng Ji, and Amanda Stent (Eds.). Association for Computational Linguistics, 474–479. <https://doi.org/10.18653/v1/n18-2076>
- [23] Daniel Libman, Simi Haber, and Mary Schaps. 2019. Volume Prediction With Neural Networks. *Frontiers in Artificial Intelligence* 2 (2019), 21. <https://doi.org/10.3389/frai.2019.00021>
- [24] Xiaotao Liu and Kin Keung Lai. 2017. Intraday volume percentages forecasting using a dynamic SVM-based approach. *Journal of Systems Science and Complexity* 30, 2 (2017), 421–433.
- [25] Thang Luong, Hieu Pham, and Christopher D. Manning. 2015. Effective Approaches to Attention-based Neural Machine Translation. In *Proceedings of the 2015 Conference on Empirical Methods in Natural Language Processing, EMNLP 2015, Lisbon, Portugal, September 17-21, 2015*, Lluís Màrquez, Chris Callison-Burch, Jian Su, Daniele Pighin, and Yuval Marton (Eds.). The Association for Computational Linguistics, 1412–1421.
- [26] Aleksander Madry, Aleksandar Makelov, Ludwig Schmidt, Dimitris Tsipras, and Adrian Vladu. 2018. Towards Deep Learning Models Resistant to Adversarial Attacks. In *6th International Conference on Learning Representations, ICLR 2018, Vancouver, BC, Canada, April 30 - May 3, 2018, Conference Track Proceedings*.
- [27] Daniel Mitchell, Jędrzej Paweł Białkowski, and Stathis Tompavidis. 2013. Optimal VWAP Tracking. *Available at SSRN 2333916* (2013).
- [28] Seyed-Mohsen Moosavi-Dezfooli, Alhussein Fawzi, Omar Fawzi, and Pascal Frossard. 2016. Universal adversarial perturbations. *CoRR abs/1610.08401* (2016). [arXiv:1610.08401](https://arxiv.org/abs/1610.08401) <http://arxiv.org/abs/1610.08401>
- [29] Seyed-Mohsen Moosavi-Dezfooli, Alhussein Fawzi, and Pascal Frossard. 2016. DeepFool: A Simple and Accurate Method to Fool Deep Neural Networks. In *2016 IEEE Conference on Computer Vision and Pattern Recognition, CVPR 2016, Las Vegas, NV, USA, June 27-30, 2016*. IEEE Computer Society, 2574–2582. <https://doi.org/10.1109/CVPR.2016.282>
- [30] Ali Shafahi, Mahyar Najibi, Amin Ghiasi, Zheng Xu, John P. Dickerson, Christoph Studer, Larry S. Davis, Gavin Taylor, and Tom Goldstein. 2019. Adversarial training for free!. In *Advances in Neural Information Processing Systems 32: Annual Conference on Neural Information Processing Systems 2019, NeurIPS 2019, December 8-14, 2019, Vancouver, BC, Canada*, Hanna M. Wallach, Hugo Larochelle, Alina Beygelzimer, Florence d’Alché-Buc, Emily B. Fox, and Roman Garnett (Eds.). 3353–3364. <https://proceedings.neurips.cc/paper/2019/hash/7503cfacd12053d309b6bed5c89de212-Abstract.html>
- [31] Uri Shaham, Yutaro Yamada, and Sahand Negahban. 2015. Understanding Adversarial Training: Increasing Local Stability of Neural Nets through Robust Optimization. *CoRR abs/1511.05432* (2015). [arXiv:1511.05432](https://arxiv.org/abs/1511.05432) <http://arxiv.org/abs/1511.05432>
- [32] Jiawei Su, Danilo Vasconcellos Vargas, and Kouichi Sakurai. 2017. One pixel attack for fooling deep neural networks. *CoRR abs/1710.08864* (2017). [arXiv:1710.08864](https://arxiv.org/abs/1710.08864) <http://arxiv.org/abs/1710.08864>
- [33] Christian Szegedy, Wojciech Zaremba, Ilya Sutskever, Joan Bruna, Dumitru Erhan, Ian J. Goodfellow, and Rob Fergus. 2014. Intriguing properties of neural networks. In *2nd International Conference on Learning Representations, ICLR 2014, Banff, AB, Canada, April 14-16, 2014, Conference Track Proceedings*.
- [34] Balázs Árpád Szűcs. 2017. Forecasting intraday volume: Comparison of two early models. *Finance Research Letters* 21 (2017), 249–258.
- [35] Ashish Vaswani, Noam Shazeer, Niki Parmar, Jakob Uszkoreit, Llion Jones, Aidan N. Gomez, Lukasz Kaiser, and Illia Polosukhin. 2017. Attention is All you Need. In *Advances in Neural Information Processing Systems 30: Annual Conference on Neural Information Processing Systems 2017, 4-9 December 2017, Long Beach, CA, USA*. 5998–6008.
- [36] J. Wang, Tianyun Zhang, S. Liu, Pin-Yu Chen, Jiachen Xu, M. Fardad, and B. Li. 2019. Towards A Unified Min-Max Framework for Adversarial Exploration and Robustness. *arXiv: Learning* (2019).
- [37] Xunyu Ye, Rui Yan, and Handong Li. 2014. Forecasting trading volume in the Chinese stock market based on the dynamic VWAP. *Studies in Nonlinear Dynamics & Econometrics* 18, 2 (2014), 125–144.
- [38] Dinghui Zhang, Tianyuan Zhang, Yiping Lu, Zhanxing Zhu, and Bin Dong. 2019. You Only Propagate Once: Accelerating Adversarial Training via Maximal Principle. In *Advances in Neural Information Processing Systems 32: Annual Conference on Neural Information Processing Systems 2019, NeurIPS 2019, 8-14 December 2019, Vancouver, BC, Canada*, Hanna M. Wallach, Hugo Larochelle, Alina Beygelzimer, Florence d’Alché-Buc, Emily B. Fox, and Roman Garnett (Eds.). 227–238.
- [39] Richard Zhang. 2019. Making Convolutional Networks Shift-Invariant Again. In *Proceedings of the 36th International Conference on Machine Learning, ICML 2019, 9-15 June 2019, Long Beach, California, USA (Proceedings of Machine Learning Research, Vol. 97)*, Kamalika Chaudhuri and Ruslan Salakhutdinov (Eds.). PMLR, 7324–7334. <http://proceedings.mlr.press/v97/zhang19a.html>
- [40] Wei Zhang, Qian Chen, and Yunfang Chen. 2020. Deep Learning Based Robust Text Classification Method via Virtual Adversarial Training. *IEEE Access* 8 (2020), 61174–61182. <https://doi.org/10.1109/ACCESS.2020.2981616>
- [41] Stephan Zheng, Yang Song, Thomas Leung, and Ian J. Goodfellow. 2016. Improving the Robustness of Deep Neural Networks via Stability Training. In *2016 IEEE Conference on Computer Vision and Pattern Recognition, CVPR 2016, Las Vegas, NV, USA, June 27-30, 2016*. IEEE Computer Society, 4480–4488. <https://doi.org/10.1109/CVPR.2016.485>

- [42] Chen Zhu, Yu Cheng, Zhe Gan, Siqi Sun, Tom Goldstein, and Jingjing Liu. 2019. FreeLB: Enhanced Adversarial Training for Language Understanding. *CoRR* abs/1909.11764 (2019). arXiv:1909.11764
- [43] Xiaotian Zhu, Hong Wang, Li Xu, and Huaizu Li. 2008. Predicting stock index increments by neural networks: The role of trading volume under different horizons. *Expert Systems with Applications* 34, 4 (2008), 3043–3054.

A THEORETICAL DETAILS

A.1 Closed-form Solutions in FGSM and PGD Algorithms after Rescaling

COROLLARY 1. *Suppose the constraint set is $S = \{\delta : \|\alpha^{-1} \circ \delta\|_p \leq \epsilon\}$, the following are the solution of the optimization problem,*

$$\delta = \arg \max_{\delta \in S} \delta^T \mathbf{g} = \epsilon (\alpha \circ \text{sgn}(\mathbf{g})) \circ \frac{|\alpha \circ \mathbf{g}|^{\frac{1}{p-1}}}{\|\alpha \circ \mathbf{g}\|_p^{\frac{1}{p-1}}} \quad (21)$$

PROOF. Suppose $\frac{1}{p} + \frac{1}{q} = 1$, according to the Holder Inequality,

$$\delta^T \mathbf{g} = (\alpha^{-1} \circ \delta)^T (\alpha \circ \mathbf{g}) \quad (22)$$

$$\leq \|\alpha^{-1} \circ \delta\|_p \|\alpha \circ \mathbf{g}\|_q = \epsilon \|\alpha \circ \mathbf{g}\|_q \quad (23)$$

The equation holds if and only if, there exists $\lambda > 0$,

$$|\alpha^{-1} \circ \delta|^p = \lambda |\alpha \circ \mathbf{g}|^q, \text{sgn}(\alpha^{-1} \circ \delta) = \text{sgn}(\alpha \circ \mathbf{g}) \quad (24)$$

that is to say,

$$\alpha^{-1} \circ \delta = \lambda \text{sgn}(\alpha \circ \mathbf{g}) \circ |\alpha \circ \mathbf{g}|^{\frac{q}{p}} \quad (25)$$

$$= \lambda \text{sgn}(\mathbf{g}) \circ |\alpha \circ \mathbf{g}|^{\frac{1}{p-1}} \quad (26)$$

According to $\|\alpha^{-1} \circ \delta\|_p = \epsilon$, we can solve the λ ,

$$\|\alpha^{-1} \circ \delta\|_p = \|\text{sgn}(\mathbf{g}) \circ \lambda |\alpha \circ \mathbf{g}|^{\frac{1}{p-1}}\|_p = \epsilon, \quad (27)$$

$$\lambda = \frac{\epsilon}{\|\alpha \circ \mathbf{g}\|_p^{\frac{1}{p-1}}} \quad (28)$$

To conclude,

$$\alpha^{-1} \circ \delta = \epsilon \text{sgn}(\mathbf{g}) \circ \frac{|\alpha \circ \mathbf{g}|^{\frac{1}{p-1}}}{\|\alpha \circ \mathbf{g}\|_p^{\frac{1}{p-1}}} \quad (29)$$

$$\delta = \epsilon (\alpha \circ \text{sgn}(\mathbf{g})) \circ \frac{|\alpha \circ \mathbf{g}|^{\frac{1}{p-1}}}{\|\alpha \circ \mathbf{g}\|_p^{\frac{1}{p-1}}} \quad (30)$$

□

COROLLARY 2. *Suppose the constraint set is $S = \{\delta : \|\alpha^{-1} \circ \delta\|_p \leq \epsilon\}$, the following are the variants of the projection functions,*

$$\Pi_{\{\mathbf{v} : \|\alpha^{-1} \circ \mathbf{v}\|_2 \leq \epsilon\}}(\mathbf{v}) = \min\{\|\alpha^{-1} \circ \mathbf{v}\|_2, \epsilon\} \frac{\mathbf{v}}{\|\alpha^{-1} \circ \mathbf{v}\|_2} \quad (31)$$

$$\Pi_{\{\mathbf{v} : \|\alpha^{-1} \circ \mathbf{v}\|_{+\infty} \leq \epsilon\}}(\mathbf{v}) = \alpha \circ \text{clip}(\alpha^{-1} \circ \mathbf{v}, -\epsilon, \epsilon) \quad (32)$$

PROOF. Define $\mathbf{u} = \alpha^{-1} \circ \mathbf{v}$, $S' = \{\mathbf{u} : \|\mathbf{u}\|_p \leq \epsilon\}$. Consider a mapping $\phi(\mathbf{v}) = \alpha \circ \mathbf{v}$, then $\phi(\mathbf{u}) = \mathbf{v}$ and $\phi(S') = S$.

Since \mathbf{u} is projected to $\Pi_{S'}(\mathbf{u})$ in S' , we adopt the variant that projects $\mathbf{v} = \phi(\mathbf{u})$ to $\phi(\Pi_{S'}(\mathbf{u}))$, namely

$$\Pi_S(\mathbf{v}) = \phi(\Pi_{S'}(\mathbf{u})) = \alpha \circ (\Pi_{S'}(\mathbf{u})) = \alpha \circ (\Pi_{S'}(\alpha^{-1} \circ \mathbf{v})) \quad (33)$$

therefore,

$$\Pi_{\{\mathbf{v} : \|\alpha^{-1} \circ \mathbf{v}\|_2 \leq \epsilon\}}(\mathbf{v}) = \min\{\|\mathbf{u}\|_2, \epsilon\} \frac{\alpha \circ \mathbf{u}}{\|\mathbf{u}\|_2} \quad (34)$$

$$= \min\{\|\alpha^{-1} \circ \mathbf{v}\|_2, \epsilon\} \frac{\mathbf{v}}{\|\alpha^{-1} \circ \mathbf{v}\|_2} \quad (35)$$

$$\Pi_{\{\mathbf{v} : \|\alpha^{-1} \circ \mathbf{v}\|_{+\infty} \leq \epsilon\}}(\mathbf{v}) = \alpha \circ \text{clip}(\mathbf{u}, -\epsilon, \epsilon) \quad (36)$$

$$= \alpha \circ \text{clip}(\alpha^{-1} \circ \mathbf{v}, -\epsilon, \epsilon) \quad (37)$$

□

A.2 Proofs of Proposition 1

PROOF. Since when $|\delta_i| \leq \epsilon$, $\delta_{\neq i} = 0$, according to Taylor series with Lagrange form of the remainder, there exists η near \mathbf{x} ,

$$\mathcal{L}(f(\mathbf{x} + \delta, \theta), y) - \mathcal{L}(f(\mathbf{x}, \theta), y) \quad (38)$$

$$= \ell'(f(\mathbf{x}, \theta))(\theta_i \delta_i) + \frac{\ell''(f(\eta, \theta))}{2} (\theta_i \delta_i)^2 \quad (39)$$

$$\max_{|\delta_i| \leq \epsilon, \delta_{\neq i} = 0} [\mathcal{L}(f(\mathbf{x} + \delta, \theta), y) - \mathcal{L}(f(\mathbf{x}, \theta), y)] \quad (40)$$

$$= |\ell'(f(\mathbf{x}, \theta))| |\theta_i| \epsilon + \frac{\ell''(f(\eta, \theta))}{2} (\theta_i \epsilon)^2 \quad (41)$$

therefore, when $C = \mathbb{E}_{(\mathbf{x}, y) \sim \mathcal{D}} |\ell'(f(\mathbf{x}, \theta))|$,

$$\mathcal{R}_i(\epsilon) = \mathbb{E}_{(\mathbf{x}, y) \sim \mathcal{D}} \left[\max_{|\delta_i| \leq \epsilon, \delta_{\neq i} = 0} \right] \quad (42)$$

$$[\mathcal{L}(f(\mathbf{x} + \delta, \theta), y) - \mathcal{L}(f(\mathbf{x}, \theta), y)] \quad (43)$$

$$= C \epsilon |\theta_i| + \frac{\mathbb{E}_{(\mathbf{x}, y) \sim \mathcal{D}} \ell''(f(\eta, \theta))}{2} (\theta_i \epsilon)^2 \quad (44)$$

$$= C \epsilon |\theta_i| + O\left(\frac{M \theta_i^2 \epsilon^2}{2}\right) \quad (45)$$

□

B DETAILS OF HYPERPARAMETERS CHOICE

We grid-search the hyperparameters ϵ in $\{0.001, 0.002, 0.005, 0.01, 0.02, 0.05, 0.1, 0.2, 0.5, 1\}$ and γ in $\{0.1, 0.2, 0.3, 0.4, 0.5, 0.6, 0.7, 0.8, 0.9, 0.95\}$ and try L_2 and $L_{+\infty}$. To investigate the influence of hyperparameters ϵ and γ , we take the Transformer model on the five-minute dataset as an example, and discuss the influence of hyperparameters ϵ and γ according to the experimental results.

B.1 The Influence of Hyperparameter ϵ

We conduct experiments to investigate the influence of hyperparameter ϵ . Experimental results are shown in Table 5, where the $L_{+\infty}$ constraint is adopted and $\gamma = 0.7$. The process of hyperparameter search shows that too large or small ϵ cannot improve the model accuracy well, and an appropriate ϵ needs to be selected.

Table 5: Experimental results of different γ in ASAT.

Settings	MSE	RMSE	MAE	ACC
20-day average	0.700	0.837	0.608	0.709
Transformer	0.665±0.044	0.815±0.027	0.610±0.032	0.695±0.019
+ASAT ($\epsilon = 0.01$)	0.659±0.073	0.811±0.044	0.607±0.055	0.691±0.033
+ASAT ($\epsilon = 0.02$)	0.613±0.028	0.783±0.018	0.571±0.018	0.717±0.007
+ASAT ($\epsilon = 0.05$)	0.632±0.036	0.795±0.022	0.586±0.055	0.708±0.010
+ASAT ($\epsilon = 0.1$)	0.634±0.024	0.796±0.015	0.589±0.016	0.707±0.007
+ASAT ($\epsilon = 0.2$)	0.736±0.074	0.857±0.043	0.658±0.045	0.676±0.024

B.2 The Influence of Hyperparameter γ

We also conduct experiments to investigate the influence of hyperparameter γ . Experimental results are shown in Table 6, where the $L_{+\infty}$ constraint is adopted and $\epsilon = 0.02$. We can conclude that too large or small γ cannot improve the model accuracy well, and an appropriate γ needs to be selected too for the same ϵ .

Table 6: Experimental results of different γ in ASAT.

Settings	MSE	RMSE	MAE	ACC
20-day average	0.700	0.837	0.608	0.709
Transformer	0.665±0.044	0.815±0.027	0.610±0.032	0.695±0.019
+ASAT ($\gamma = 0.5$)	0.658±0.086	0.810±0.052	0.605±0.065	0.696±0.037
+ASAT ($\gamma = 0.6$)	0.666±0.063	0.815±0.038	0.614±0.048	0.691±0.038
+ASAT ($\gamma = 0.7$)	0.613±0.028	0.783±0.018	0.571±0.018	0.717±0.007
+ASAT ($\gamma = 0.8$)	0.618±0.032	0.786±0.020	0.574±0.019	0.716±0.009
+ASAT ($\gamma = 0.9$)	0.670±0.086	0.817±0.051	0.614±0.064	0.691±0.068

B.3 Detailed Hyperparameters Settings

We conduct hyperparameter search experiments to find the best configurations of hyperparameters.

We first report the best configurations on the hourly dataset. On the linear model, we adopt the $L_{+\infty}$ constraint, $\epsilon = 0.01$, and $\gamma = 0.1$. On the LSTM model, we adopt the $L_{+\infty}$ constraint, $\epsilon = 0.1$, and $\gamma = 0.7$. On the Transformer model, we adopt the L_2 constraint, $\epsilon = 0.05$, and $\gamma = 0.5$.

We then report the best configurations on the five-minute dataset. On the linear model, we adopt the $L_{+\infty}$ constraint, $\epsilon = 0.1$, and $\gamma = 0.95$. On the LSTM model, we adopt the L_2 constraint, $\epsilon = 0.5$, and $\gamma = 0.9$. On the Transformer model, we adopt the $L_{+\infty}$ constraint, $\epsilon = 0.02$, and $\gamma = 0.7$.